

ELECTRON BEAM AS ORIGIN OF WHITE-LIGHT SOLAR FLARES

J. ABOUDARHAM and J. C. HENOUX

DASOP, Observatoire de Paris-Meudon, 92195 Meudon Principal Cedex, France

Abstract. We study the effect of chromospheric bombardment by an electron beam during solar flares. Using a semi-empirical flare model, we investigate energy balance at temperature minimum level and in the upper photosphere. We show that non-thermal hydrogen ionization (i.e., due to the electrons of the beam) leads to an increase of chromospheric hydrogen continuum emission, H^- population, and absorption of photospheric and chromospheric continuum radiation. So, the upper photosphere is radiatively heated by chromospheric continuum radiation produced by the beam. The effect of hydrogen ionization is an enhanced white-light emission both at chromospheric and photospheric level, due to Paschen and H^- continua emission, respectively. We then obtain white-light contrasts compatible with observations, obviously showing the link between white-light flares and atmospheric bombardment by electron beams.

1. Introduction

White-light flares (WLF) are characterized by an increase in emission in the visible range. It has been deduced from observations that the source of this emission is placed in the low atmosphere: low chromosphere and upper photosphere, showing a heating of these layers during the flare. It is important to determine whether this temperature increase can be explained by energy transport from the lower corona, or whether it requires a partial or total *in situ* energy release.

The two main contributors of white-light emission are negative hydrogen, originating in the upper photosphere (see Neidig, 1983, for instance), and Paschen recombination continuum from chromospheric origin.

Hudson (1972) suggested a link between WLF and atmospheric bombardment by beams, proton, or electron beams. But none of these seem to be able to explain the observed low atmosphere heating: protons, which could penetrate deeply in the atmosphere, must be over 100 MeV in order to reach the photosphere and then must emit γ -emission which is not systematically correlated with WLF; and electrons do not seem to be able to deposit enough energy in the upper photosphere. But, due to the lack of detailed calculations, it was impossible to remove doubt.

In Section 2, we shall show what makes the electron beam a good applicant for WLF, deduced from hard X-ray observations.

Section 3 is devoted to the detailed calculation concerning both an electron beam and the flaring atmosphere. We first derived the energy deposited by the beam along its way through the atmosphere. From this, we deduced hydrogen excitation and ionization rates due to the electrons of the beam, what we call 'non-thermal' collisional rates. The semi-empirical flare model F_2 (Machado *et al.*, 1980), giving temperature distribution versus column mass for a strong flare was used in order to estimate the thermal

collisional excitation and ionization rates. The quiet-Sun model *C* (Vernazza, Avrett, and Loeser, 1981) was used as a reference, for the 'background' Sun, necessary in the calculation of the energy input present in the quiet-Sun conditions and of the contrast during the flare. We then studied the atmospheric response, solving radiative transfer, statistical equilibrium and electrical neutrality equations, leading to the determination of radiative losses and thermal (i.e., due to background electrons) excitation and ionization rates. In Section 4 we show that non-thermal rates should not be neglected. Their contribution leads to an increase in electron density which enhances Paschen continuum emission and H^- absorption. Consequently, the upper photosphere as represented by semi-empirical flare model F_2 is not in energetic equilibrium. When the initial total energy flux of the electron beam is 10^{12} ergs $\text{cm}^{-2} \text{s}^{-1}$, energy balance in the upper photosphere is reached by increasing the upper photosphere temperature by approximately 240 K.

This radiative heating of the low atmosphere during flares leads to a strong white-light contrast which can now account for WLF observations.

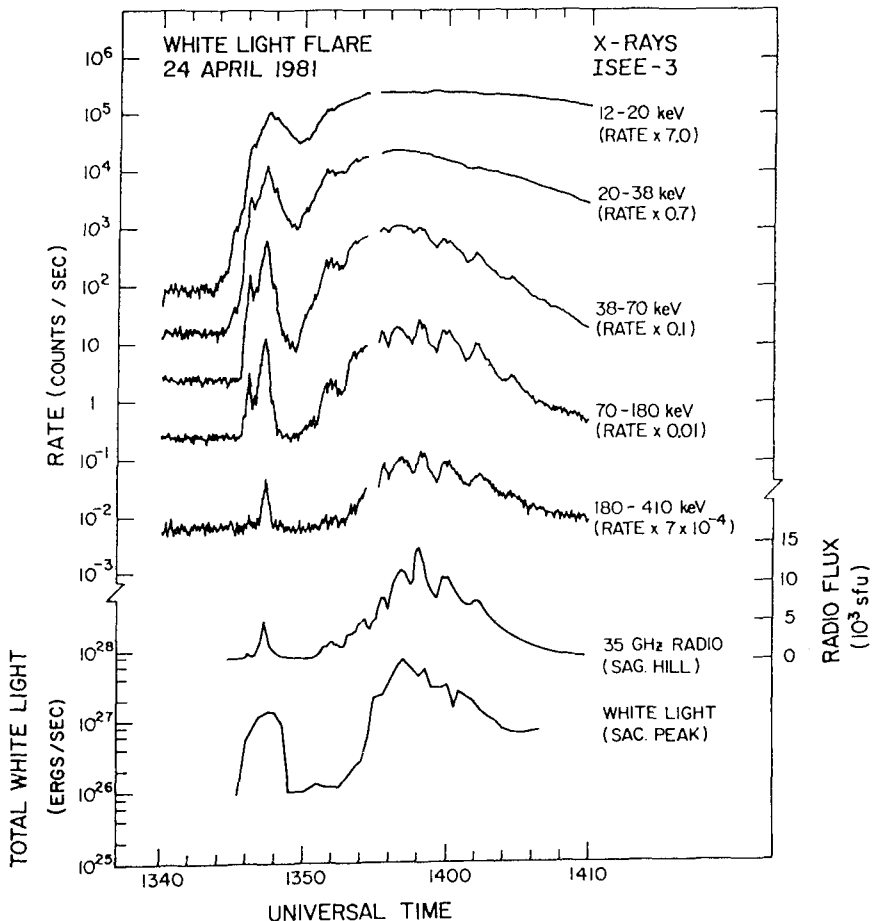


Fig. 1. Time-correlation between hard X-ray and white-light emission (from Kane *et al.*, 1985).

2. An Approach of the WLF Problem

Simultaneous observations of hard X-ray and white-light emissions show a very good time-correlation between their impulsive phases, as shown in Figure 1. This means the mechanisms leading to those emissions are connected. It is generally believed that hard X-ray emission is produced by collisional bremsstrahlung of non-thermal electrons accelerated in the low corona and slowed down in the denser chromosphere (see Brown, 1973, for instance). The best observed time-correlations between hard X-ray and white light emission are for photons of energy greater than ≈ 70 keV, and only electrons of energy above 70 keV can reach chromosphere. We can then speculate that the chromospheric bombardment by an electron beam is, at least, somewhat responsible for white-light emission. The hard X-ray emission is fitted by a power-law distribution in energy with a spectral index γ ; so, using the thick-target approximation, the electron flux is also represented by a power-law distribution with a spectral index δ which is related to γ the following way (Brown, 1972):

$$\delta = \gamma + 1.$$

Then, in the weakly ionized low chromosphere and upper photosphere, the electrons of the beam lose their energy in collisions with neutral atoms, thus exciting and ionizing neutral hydrogen of the chromosphere.

3. Calculation

3.1. BEAM EXCITATION AND IONIZATION OF THE ATMOSPHERE

The rate of energy deposited by the electrons of the beam in collisional excitation and ionization of neutral hydrogen is given by (Emslie, 1978; Chambe and Hénoux, 1979)

$$\begin{aligned} \frac{dE^H}{dt} \text{ (erg cm}^{-2} \text{ s}^{-1}\text{)} &= \\ &= \frac{1}{2}(1-x)n_H A' \frac{K \mathcal{F}_1}{E_1} \left(\frac{N}{N_1}\right)^{-\delta/2} (\delta-2) \int_0^{u_1} \frac{u^{(\delta/2)-1}}{(1-u)^{(2+\bar{\beta})/(4+\bar{\beta})}} du. \end{aligned} \quad (1)$$

The electron flux is represented by a power law $\mathcal{F} \sim E^{-\delta}$ with a low-energy cut-off E_1 . \mathcal{F}_1 is the total energy flux above E_1 and N_1 is the hydrogen column density at the deepest level electrons of energy E_1 can reach. A given column density N can only be penetrated by electrons of initial energy greater than

$$E_N = \left[\left(2 + \frac{\bar{\beta}}{2} \right) \frac{\bar{\gamma} KN}{\mu_0} \right]^{1/2}, \quad (2)$$

where μ_0 is the cosine of the angle between the initial velocity vector and the solar vertical; $K = 2\pi e^4$; $\bar{\beta}$ and $\bar{\gamma}$ are the mean values along the electron trajectory of β and

γ , given by

$$\beta = \frac{2xA + (1-x)(A' + A'')}{x(A - A') + A'}, \quad \gamma = xA + (1-x)A', \quad (3)$$

A , A' , and A'' are specified in Emslie's paper. A represents the effects of the collisions of the electrons of the beam on the ambient free electrons and protons; A' and A'' the effects of the inelastic and elastic collisions, respectively, on neutral hydrogen atoms; x is the hydrogen ionization degree

$$u = (E_N/E)^2,$$

where E is the electron energy, and

$$u_1 = 1, \quad N > N_1,$$

$$u_1 = (N/N_1), \quad N \leq N_1.$$

The electrons of the beam lose their energy in elastic collisions with electrons and inelastic collisions with neutral hydrogen. The latter correspond mainly to excitation of levels $n = 2$ and $n = 3$ and to ionization of hydrogen. Therefore, the rate of energy deposit due to collisions with neutral hydrogen is directly related to the non-thermal excitation rates, to levels 2 and 3, and ionization rate:

$$\frac{dE^H}{dt} \text{ (eV s}^{-1}\text{)} \simeq n_1(\chi_{12}C_{12}^B + \chi_{13}C_{13}^B + \chi_{1c}C_{1c}^B), \quad (4)$$

where dE^H/dt is the rate of energy deposit due to collisions with hydrogen. C_{12}^B , C_{13}^B , and C_{1c}^B are, respectively, the excitation rates to levels 2 and 3 and the ionization rate due to the electron beam. χ_{12} , χ_{13} , and χ_{1c} are excitation potential of levels 2 and 3, and ionization potential, respectively. The non-thermal rates C_{ij}^B are, as an approximation, proportional to excitation and ionization cross-sections of hydrogen by 10–100 keV electrons. Mott and Massey (1965) give the relative importance of these terms: respectively, 0.53, 0.08, 0.39, leading to the following expressions of non-thermal excitation and ionization rates:

$$C_{12}^B = 2.77 \times 10^{10} \frac{dE^H}{dt}, \quad C_{13}^B = 0.15C_{12}^B, \quad C_{1c}^B = 0.74C_{12}^B.$$

3.2. THERMAL EXCITATION AND IONIZATION OF THE ATMOSPHERE

A plane-parallel atmosphere representation of the solar chromosphere can be adopted to describe the main features of the energy transport process during solar flares. We used semi-empirical flare model F_2 (Machado *et al.*, 1980), which represents a bright flare. The non-flaring atmosphere has been represented by the quiet-Sun model C (Vernazza, Avrett, and Loeser, 1981). Temperature distribution of models C and F_2 is shown in Figure 2. Temperature minimum for models C and F_2 , respectively, 4165 K and 4960 K.

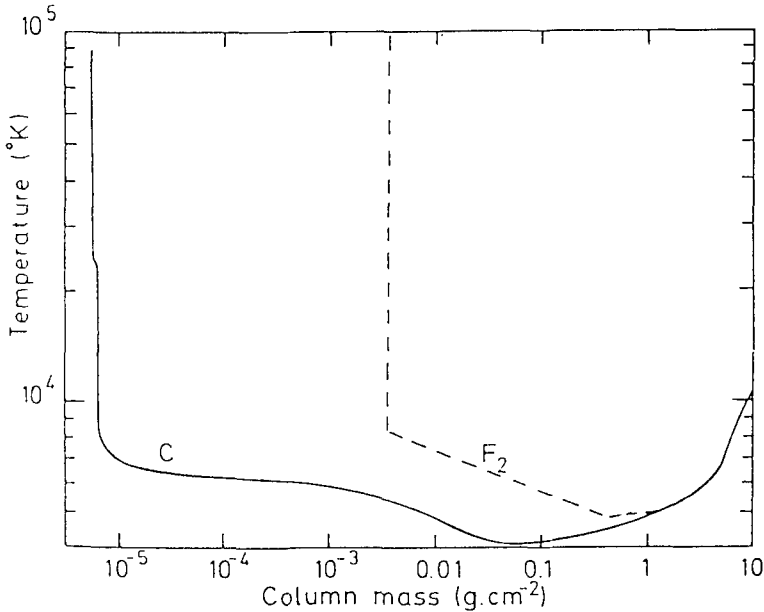


Fig. 2. Temperature distribution for the quiet Sun (model C) and for bright flares (model F_2).

From these models, we computed the non-LTE populations of H^- and of the three first levels of hydrogen by solving the transfer equation for Balmer α , Lyman α , and Lyman β lines, and for Lyman, Balmer, Paschen, and Brackett continua, and the equation of statistical equilibrium (Abouadarham, 1986). The fourth level was supposed to be in LTE. Feautrier's (1964) method was used.

Thermal collisional excitation and ionization rates C_{ij} have been deduced from this computation. We then included non-thermal processes in statistical equilibrium equation. Their effect will be described in the next section. We also calculated radiative losses for H and H^- , the latter being the main contributor at temperature minimum region (TMR) and below (Avrett, 1980, 1985). Bound-free and free-free H^- cooling rates were computed:

$$\Phi_{H_{bf}} = 4\pi n_{H^-} \int \chi_{bf}(S_\nu - J_\nu) d\nu, \quad (5)$$

$$\Phi_{H_{ff}} = 4\pi n_{H^-} \int \chi_{ff} \left[n_{H^-}^* / n_{H^-} \left(\frac{2h\nu^3}{c^2} + J_\nu \right) e^{-h\nu/kT} - J_\nu \right] d\nu, \quad (5)$$

where n_{H^-} and $n_{H^-}^*$ are H^- number density in the non-LTE and LTE case, respectively. A detailed study of H^- can be found in Abouadarham and Hénoux (1986a, 1987). We can then estimate the total amount of energy deposit $\Delta\Phi$, due to both H and H^- , required to heat the concerned regions to flare temperatures. It is supposed that the

energy deposit, that takes place in the average quiet Sun, does not vary from quiet Sun to flare conditions. In addition to this, we assume the energy deposit depends only on column mass m . Then the additional energy deposit $\Delta\Phi$ required, at column mass m , to increase quiet-Sun temperature to flare temperature is given by

$$\Delta\Phi_{F_2C} = \Phi_{F_2}(m) - \Phi_C(m), \tag{6}$$

where $\Phi_{F_2}(m)$ and $\Phi_C(m)$ are, respectively, the radiative losses per unit volume inferred from model F_2 and model C .

4. Results: Beam Effect on the Atmosphere

4.1. BEAM CHARACTERISTICS AND EFFECTS ON HYDROGEN

The main features characterizing the energy deposited by the beam, as shown in Equation (1), are low-energy cut-off, E_1 , initial flux above E_1 , \mathcal{F}_1 , and spectral index, δ . The standard value of 20 keV for the low-energy cut-off was adopted and the total energy flux \mathcal{F}_1 above 20 keV is 10^{12} ergs $\text{cm}^{-2} \text{s}^{-1}$. The chosen spectral index is $\delta = 4$. Those values were adopted according to the fact model F_2 represents a strong flare. Discussion on these values can be found in Aboudarham and Hénoux (1986b). In fact, only electrons of energy greater than 70 keV can reach chromosphere; this leads to an energy flux of 8×10^{10} ergs $\text{cm}^{-2} \text{s}^{-1}$ above 70 keV.

Figure 3 shows thermal collisional excitation and ionization rates and non-thermal

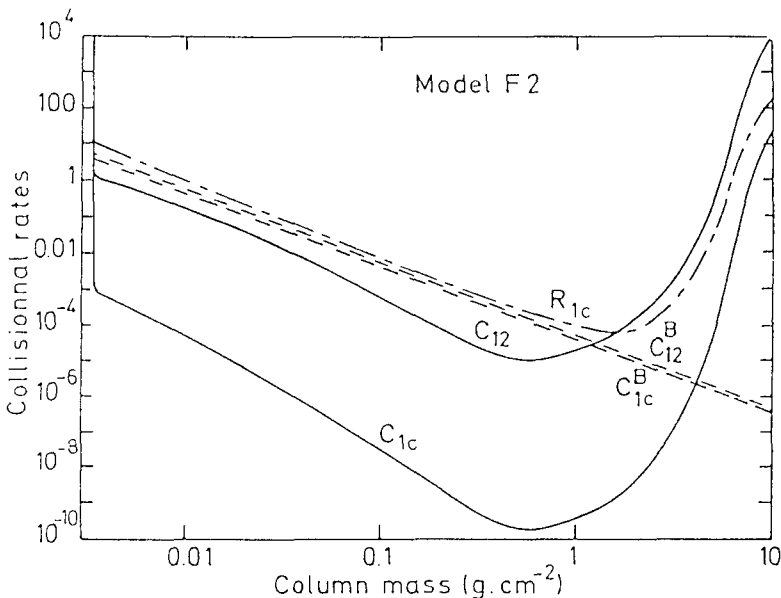


Fig. 3. Collisional excitation rate of hydrogen level 2 and collisional and radiative ionization rates of hydrogen as a function of column mass. Full lines: thermal collisional rates. Dashed lines: non-thermal collisional rates. Dotted-dashed line: photoionization rate.

ones, according to the above values characterizing the beam. We can see that non-thermal rates are much stronger than thermal ones, especially for non-thermal ionization rate which is four to six orders of magnitude higher than the thermal ionization rate in the middle chromosphere and below. This means that a detailed flaring atmosphere calculation should not neglect non-thermal processes, even for initial energy flux in the beam several orders of magnitude lower than 10^{12} ergs cm^{-2} s^{-1} .

Non-thermal ionization increases the electron number density and decreases the hydrogen level 1 population. This makes the LTE departure coefficient for levels 1, 2, 3 of hydrogen decrease. Source functions in continua decrease, leading to enhanced radiative losses, especially in the Paschen continuum, as shown in Figure 4. This enhancement of the chromospheric Paschen emission should lead to an increase in the white light emission.

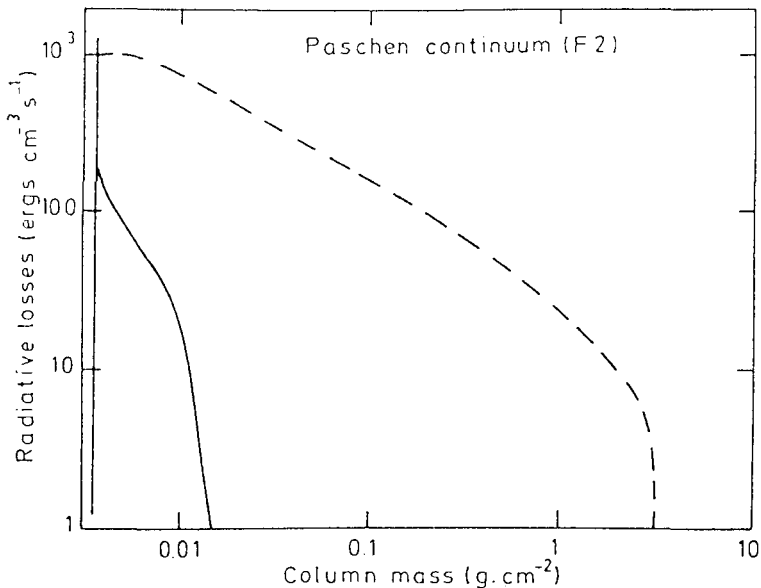


Fig. 4. Column mass dependence of the hydrogen Paschen continuum emission. Full line: without non-thermal collisional excitation and ionization. Dashed line: non-thermal collisional excitation and ionization included.

4.2. EFFECT ON TOTAL RADIATIVE LOSSES

Figure 5 shows the column mass dependence of the difference of the total radiative losses ($\text{H} + \text{H}^-$), $\Delta\Phi_{F_2C}$ (Equation (6)), calculated from models F_2 and C . We shall only examine the radiative losses below temperature minimum, where H^- originates. For a detailed discussion on chromospheric radiative losses, see Aboudarham and Hénoux (1986b).

The increase of the electron number density leads to an increase of the H^- number density. When the photoionization rate exceeds the recombination rate, H^- absorbs

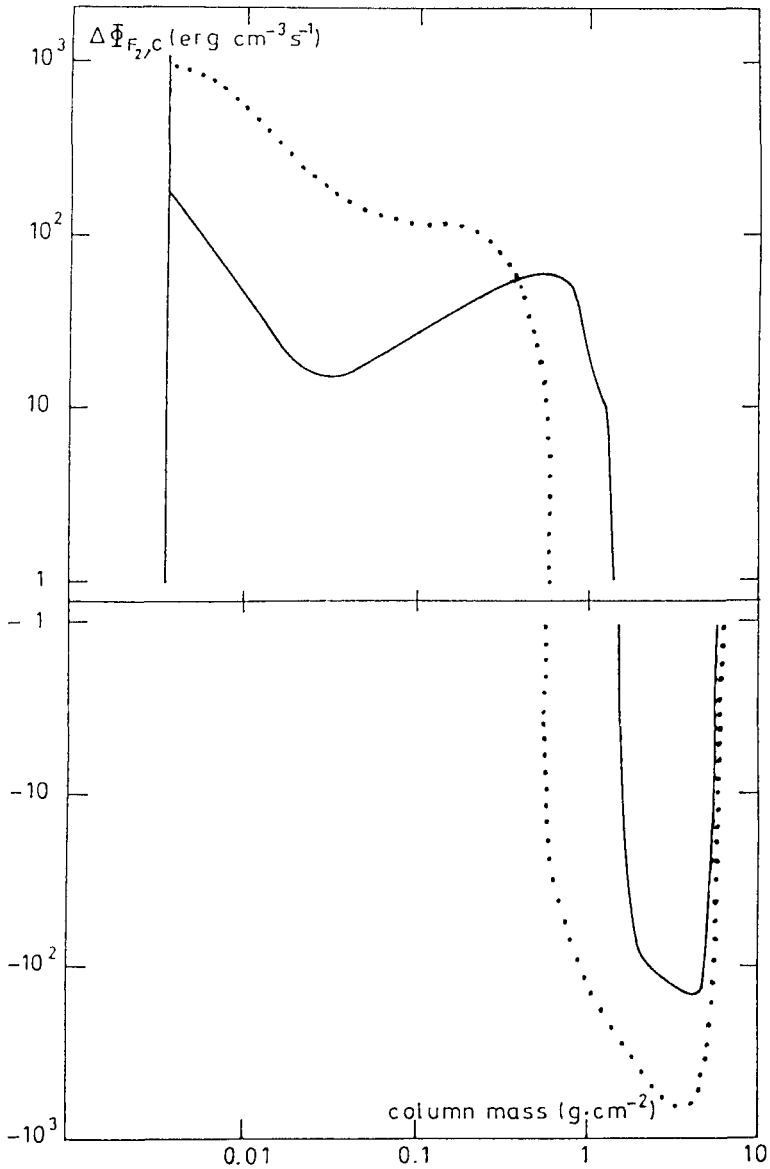


Fig. 5. Column mass dependence of $\Delta\Phi_{F_2,C}(m)$, difference of the radiative losses ($H + H^-$) of models F_2 and C . Full line: non-thermal hydrogen excitation and ionization not included. Dotted line: non-thermal hydrogen excitation and ionization included ($\mathcal{F}_1 = 10^{12}$ ergs $\text{cm}^{-2} \text{s}^{-1}$).

more radiation in the bound-free continuum than it radiates, and the total H^- radiative losses are negative. At constant temperature, density of neutral hydrogen and radiation field, the amplitude of the bound-free cooling rate increases with electron number density. So, as we can see in Figure 5, the energy input required to heat the atmosphere from quiet Sun to flare temperatures becomes more negative at column masses between

0.6 and 6 g cm^{-2} . This means that departure from energy balance becomes stronger at this level. This implies that, when taking into account non-thermal processes due to an electron beam, the temperature of the upper photosphere at this depth must increase for the atmosphere to be in energy balance. Temperature enhancement as high as 240 K is produced at column mass $m = 2 \text{ g cm}^{-2}$, as shown in Figure 6.

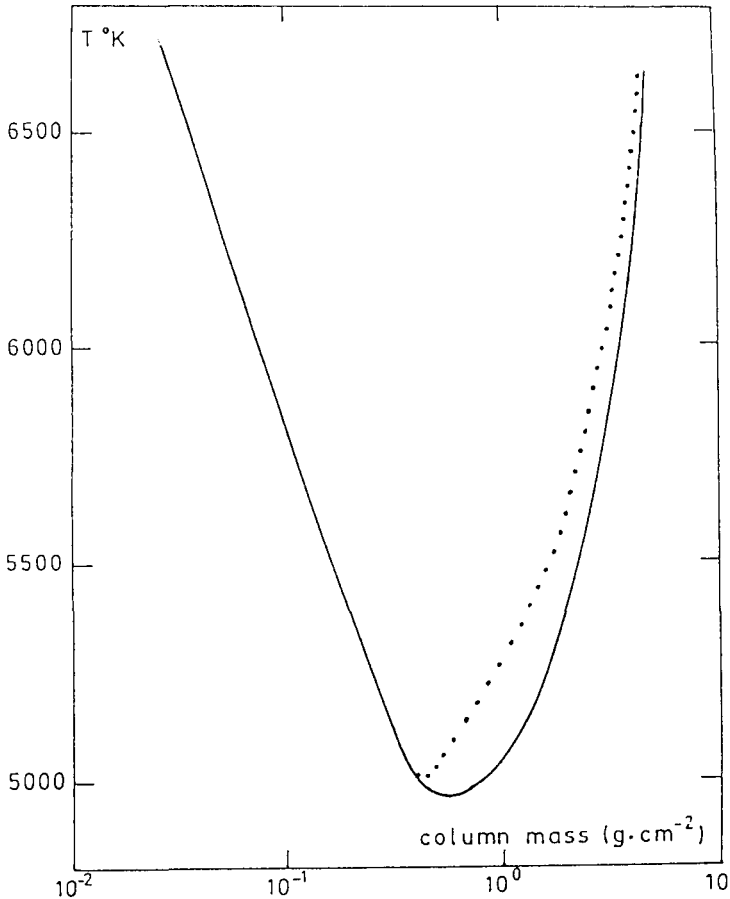


Fig. 6. Temperature distribution illustrating the upper photospheric heating induced by non-thermal processes. Full line: semi-empirical flare model F_2 . Dotted line: modified temperature distribution leading to photospheric energy balance.

4.3. EFFECT ON CONTRAST

The enhancement of both chromospheric Paschen emission and upper photospheric H^- emission due to the increase of the photospheric temperature leads to an increase of the white-light continuum emission. This is quantitatively represented by the contrast C_v , defined as

$$C_v = \frac{I_v^{F_2} - I_v^C}{I_v^C},$$

where $I_v^{F_2}$ and I_v^C are, respectively, the specific intensity inferred from model C and model F_2 . Figure 7 shows the contrast in the visible range when photospheric radiative back-heating is not taken into account and when photospheric temperature enhancement deduced from the beam is included, compared to an observation by Neidig (1983, Figure 5, p. 293) of the 24 April, 1981 flare. Note that Neidig's observed contrast is not relative to quiet-Sun intensity, but to the mean intensity averaged over lines and continua in the wavelength region of the measurements. So, the observed contrast has been recalculated (Neidig, 1988) in quiet-Sun units, as a function of wavelength. As suggested by Neidig (1988), the spectral shape of the observed contrast might be due to atmospheric

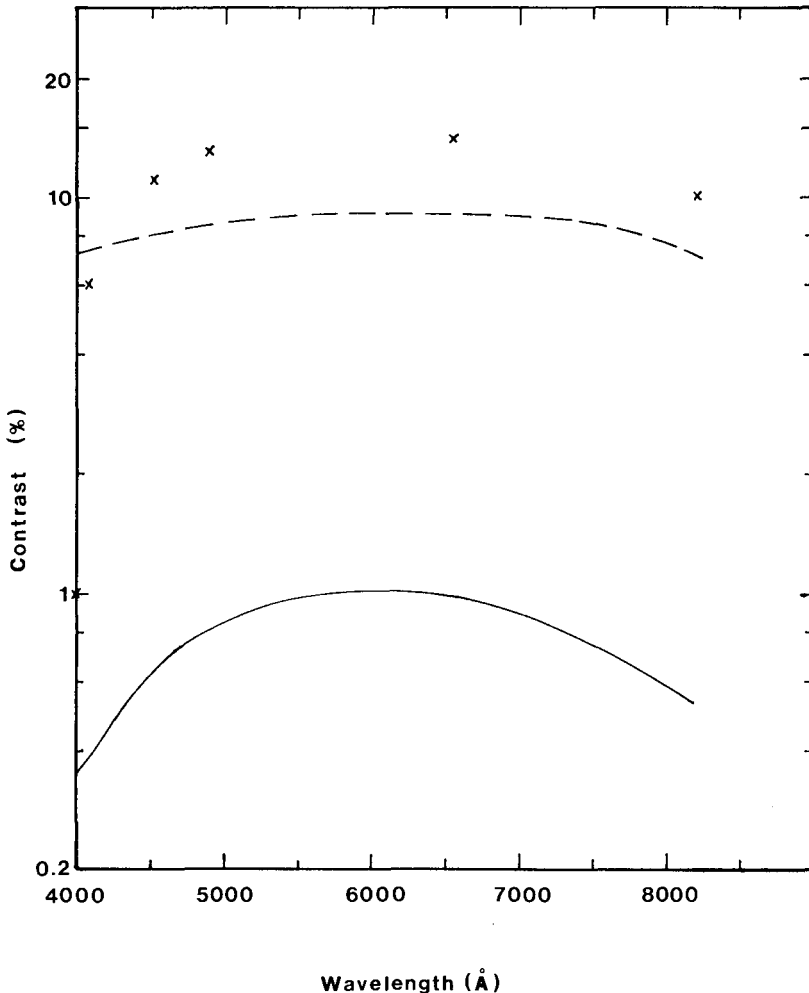


Fig. 7. Wavelength dependence of contrast C_v between flare and quiet-Sun specific intensities, for heliocentric angle $\Theta = 53^\circ$ ($\mu = \cos \Theta = 0.6$). Full line: non-thermal processes not included. Dashed line: non-thermal processes included. Crosses: observation by Neidig (1983) of 24 April, 1981 flare, modified data (see text).

refraction moving the flare image across the spectrograph slit, so that we see a progressively fainter part of the flare at shorter wavelength. It is obvious, in Figure 7, that only the inclusion of non-thermal processes due to the electrons of the beam can explain the observed white-light emission, thus demonstrating the link between electron beams and white-light flares.

5. Discussion and Conclusion

Some observations show a very strong white-light contrast which cannot be explained with our calculations, except at large heliocentric angles. In fact, they are probably overestimated, due to two reasons: first, contrast is often measured with filters that include line contribution to the total intensity. Second, the very important broadening of chromospheric Balmer lines during flares interfere strongly with visible continuum emission.

Hudson (1972) suggested that the white-light emission observed in WLF resulted from the enhancement of the hydrogen recombination spectrum due to the increase of the hydrogen ionization by collision with non-thermal electrons. Indeed, the exact computation of the white-light hydrogen and H^- spectrum shows a significant increase of this emission due to a rise of the electron number density. The resulting increase of H^- population leads to an enhanced absorption of continuum radiation. This produces both photospheric radiative heating and an upward shift of the depth of formation of H^- radiation. These processes have opposite consequences and are time-dependent. On a short time, they may produce a decrease of the net radiation field, like negative flares observed on stars. But later on the upper photosphere radiative heating, together with the increased hydrogen recombination emission, generates a white-light flare. The main driver of the white-light emission is the hydrogen non-thermal ionization, and the dominance of the non-thermal processes over the thermal ones makes this conclusion quite independent of the assumed chromospheric temperature distribution.

An electron beam of initial energy flux $\mathcal{F}_1 = 10^{12} \text{ ergs cm}^{-2} \text{ s}^{-1}$ above the standard 20 keV low-energy cut-off with a spectral index $\delta = 4$ induces an average temperature enhancement in upper photosphere ($0.6 < m < 6 \text{ g cm}^{-2}$) of 240 K, leading to a white-light contrast in good agreement with observations, demonstrating that WLF can be explained by an electron bombardment of the atmosphere during the flare, and explaining the time-correlation between hard X-ray and white-light emissions.

Acknowledgements

The authors wish to thank Dr D. F. Neidig for helpful comments and for re-calculating contrast of the 24 April, 1981 flare in quiet-Sun units in order to allow us to make comparisons with our computation, as mentioned in Section 4.3.

References

- Abouardham, J.: 1986, Ph.D. Thesis, Univ. Paris VI.
- Abouardham, J. and Hénoùx, J. C.: 1986a, *Astron. Astrophys.* **156**, 73.
- Abouardham, J. and Hénoùx, J. C.: 1986b, *Astron. Astrophys.* **168**, 301.
- Abouardham, J. and Hénoùx, J. C.: 1987, *Astron. Astrophys.* **174**, 270.
- Avrett, E. H.: 1980, in R. M. Bonnet and A. K. Dupree (eds.), *Solar Phenomena in Stars and Stellar System*, D. Reidel Publ. Co., Dordrecht, Holland.
- Avrett, E. H.: 1985, in B. W. Lites (ed.), *Chromospheric Diagnostic and Modeling*, NSO, Sunspot, NM.
- Brown, J. C.: 1972, *Solar Phys.* **26**, 441.
- Brown, J. C.: 1973, *Solar Phys.* **28**, 151.
- Chambe, G. and Hénoùx, J. C.: 1979, *Astron. Astrophys.* **80**, 123.
- Emslie, A. G.: 1978, *Astrophys. J.* **224**, 241.
- Feautrier, P.: 1964, *Compt. Rend. Acad. Sci. Paris* **258**, 3189.
- Hudson, H. S.: 1972, *Solar Phys.* **24**, 414.
- Kane, S. R., Love, J. J., Neidig, D. F., and Cliver, E. W.: 1985, *Astrophys. J.* **290**, L45.
- Machado, M. E., Avrett, E. H., Vernazza, J. E., and Noyes, R. W.: 1980, *Astrophys. J.* **242**, 336.
- Mott, N. F. and Massey, H. S. W.: 1965, *The Theory of Atomic Collisions*, Clarendon Press, Oxford.
- Neidig, D. F.: 1983, *Solar Phys.* **85**, 285.
- Neidig, D. F.: 1988, private communication.
- Vernazza, J. E., Avrett, E. H., and Loeser, R.: 1981, *Astrophys. J. Suppl.* **45**, 635.